








Review

# Magnetic Recording of Superconducting States

Gorky Shaw <sup>1,†,‡</sup> , Sylvain Blanco Alvarez <sup>1,‡</sup>, Jérémy Brisbois <sup>1,‡</sup>, Loïc Burger <sup>2</sup>,  
Lincoln B. L. G. Pinheiro <sup>3,4</sup> , Roman B. G. Kramer <sup>5</sup> , Maycon Motta <sup>3</sup> , Karl Fleury-Frenette <sup>6</sup>,  
Wilson Aires Ortiz <sup>3</sup> , Benoît Vanderheyden <sup>2</sup>  and Alejandro V. Silhanek <sup>1,\*</sup> 

<sup>1</sup> Experimental Physics of Nanostructured Materials, Q-MAT, CESAM, Université de Liège, B-4000 Sart Tilman, Belgium; gorkyshaw1984@gmail.com (G.S.); s.blanco@uliege.be (S.B.A.); jbrisbois@uliege.be (J.B.)

<sup>2</sup> SUPRATECS group, Montefiore Research Unit, Department of Electrical Engineering and Computer Science, Université de Liège, 4000 Sart Tilman, Belgium; lburger@uliege.be (L.B.); B.Vanderheyden@uliege.be (B.V.)

<sup>3</sup> Departamento de Física, Universidade Federal de São Carlos, 13565-905 São Carlos, Brazil; pinheiroblg@gmail.com (L.B.L.G.P.); m.motta@df.ufscar.br (M.M.); wortiz@df.ufscar.br (W.A.O.)

<sup>4</sup> IFSP—Instituto Federal de São Paulo, Campus São Carlos, 13.565-905 São Carlos, Brazil

<sup>5</sup> CNRS, Institut Néel, University Grenoble Alpes, 38000 Grenoble, France; roman.kramer@neel.cnrs.fr

<sup>6</sup> Centre Spatial de Liège (CSL), STAR Research Unit, Université de Liège, Liège Science Park, B-4031 Angleur, Belgium; kfleury@uliege.be

\* Correspondence: asilhanek@uliege.be; Tel.: +32-4-366-3632

† Current address: School of Applied Sciences (Physics), Kalinga Institute of Industrial Technology (Deemed to be University), Bhubaneswar, 751024 Odisha, India.

‡ These authors contributed equally to this work.

Received: 20 August 2019; Accepted: 16 September 2019; Published: 20 September 2019



**Abstract:** Local polarization of magnetic materials has become a well-known and widely used method for storing binary information. Numerous applications in our daily life such as credit cards, computer hard drives, and the popular magnetic drawing board toy, rely on this principle. In this work, we review the recent advances on the magnetic recording of inhomogeneous magnetic landscapes produced by superconducting films. We summarize the current compelling experimental evidence showing that magnetic recording can be applied for imprinting in a soft magnetic layer the flux trajectory taking place in a superconducting layer at cryogenic temperatures. This approach enables the *ex-situ* observation at room temperature of the imprinted magnetic flux landscape obtained below the critical temperature of the superconducting state. The undeniable appeal of the proposed technique lies in its simplicity and the potential to improve the spatial resolution, possibly down to the scale of a few vortices.

**Keywords:** superconductor-ferromagnet hybrids; magnetic tweezers; superconducting devices

## 1. Introduction

Superconductivity and magnetic order are two macroscopic quantum coherent states of antagonistic nature, hence, leading to competing ground states [1–3]. This competition manifests itself in the scarceness of compounds exhibiting coexistence between long-range magnetic order and superconductivity [4–8], and is also reflected in the phase diagram of cuprate superconductors where an antiferromagnetic phase develops at the expense of the superconducting phase [9,10]. The preservation of both states can be achieved by renouncing intimate coexistence and physically separating them in different layers. Yet in this case, profound modifications of the superconducting state are observed at the interface between the two materials. Even if an insulating material prevents such an interface, a mutual magnetic interaction persists through their stray fields [11]. The resulting

hybrid structures have revealed a plethora of interesting effects, such as shrinkage of magnetic domains in a ferromagnetic layer (FL) in close proximity to a superconducting layer (SL) [12] and the possibility to confine superconductivity within a narrow region on top of magnetic domain walls [13–15]. In addition, hybrid systems have found their place in numerous applications such as in magnetic cloaking metamaterials [16], for improving the critical current density in superconductors [17], and have been proposed as possible candidates for use as information storage devices [18]. In the present review we are aiming at discussing the recent theoretical and experimental progress achieved in the magnetic recording of the inhomogeneous superconducting state in superconductor/ferromagnet (S/F) hybrid structures dominated by electromagnetic interactions (i.e., orbital effect). This work is organized as follows: in Section 2 we present the pioneer reports discussing the irreversible traces of moving flux quanta on a nearby ferromagnetic layer. The associated increase of vortex damping is addressed in Section 3. Section 4 summarizes the current experimental evidence of magnetic imprinting. In the last Section 5 we draw the conclusion and formulate a number of possible issues that remain unsettled and deserve further investigation.

## 2. Superconducting Vortices as Magnetic Tweezers

In 2005, Jankó and co-workers proposed the captivating idea of using superconducting vortices, each carrying a quantum of flux, as tiny scribes able to locally polarize a nearby paramagnetic layer [19]. In their proposal, they resorted to diluted magnetic semiconductors (DMS) as the magnetic subsystem (see Figure 1) where a giant effective  $g$ -factor resulting from the exchange interaction between the  $sp$  band carriers and localized  $d$  moments, led to an unusually large Zeeman splitting [20]. In this system, the charge distribution bound at the DMS layer by the stray field of the vortex is made predominantly of carriers with their spin aligned with the vortex stray field. Although the original idea was to operate such a device within the paramagnetic regime of the DMS, *a priori* there was no reason to rule out its functionality in the ferromagnetic phase as long as the coercive field remained below the typical stray field strength of a superconducting vortex. For a superconducting film of thickness  $d$  and penetration depth  $\lambda$ , the  $z$ -component of the magnetic field strength at a distance  $z$  above the film surface produced by an isolated vortex can be estimated as [21,22],

$$B_z(r, z) = \frac{\Phi_0}{2\pi} \frac{z + \lambda_{\text{eff}}}{(r^2 + (z + \lambda_{\text{eff}})^2)^{3/2}} \leq 2H_{c1} \quad (1)$$

where  $\lambda_{\text{eff}} = \lambda \coth(d/2\lambda)$ ,  $r$  is the radial coordinate from the axis of the vortex,  $\Phi_0$  is the magnetic flux quantum, and  $H_{c1}$  is the lower critical field.

As a DMS layer, III-Mn-V materials, the more established II-Mn-VI, as well as the emerging Mn-containing group-IV alloys, could in principle be used to engineer spin-polarized charge-carrier states with specific features. Test devices producing the required non-uniform magnetic fields with nanoscale spatial variation could be readily obtained by introducing nanomagnets of various shapes [23–25] at the expense of having a rigid structure which offers no flexibility for manipulation after fabrication. However, to the best of our knowledge, an experimental corroboration of these theoretical predictions is still lacking. Among the difficulties appearing in these systems, the substantial strain fields due the lattice mismatch between the nanostructured magnetic dots or the superconducting layer and the DMS layer could override the effects produced by the inhomogeneous magnetic field. In addition, inducing spin-charge textures requires low temperature paramagnetic DMS with long mean free path, which is challenging for the III-Mn-V compounds, but could be feasible with epitaxially grown (Cd,Mn)Te quantum wells. In a study of adiabatic spin propagation in (Cd,Mn)Te quantum wells guided by helical stray magnetic field ( $\sim 50$  mT amplitude) generated by a grating of ferromagnetic stripes, Betthausen and co-workers [26] demonstrated that a large  $g$ -factor is sustained only at very low temperatures as the dominant  $s$ - $d$  exchange part in the  $g$ -factor contributes appreciably below 1 K.

Superconductor/semiconductor heterostructures (without a magnetic semiconductor) have been originally investigated experimentally by G. H. Kruithof and co-workers [27] and showed clear evidence of a strong interaction between moving flux lines and the two-dimensional electron gas. These studies have motivated Danckwerts and co-workers [28] to demonstrate that an enhanced fluxon damping produced by eddy currents in the semiconductor results from the coupling between these two subsystems.

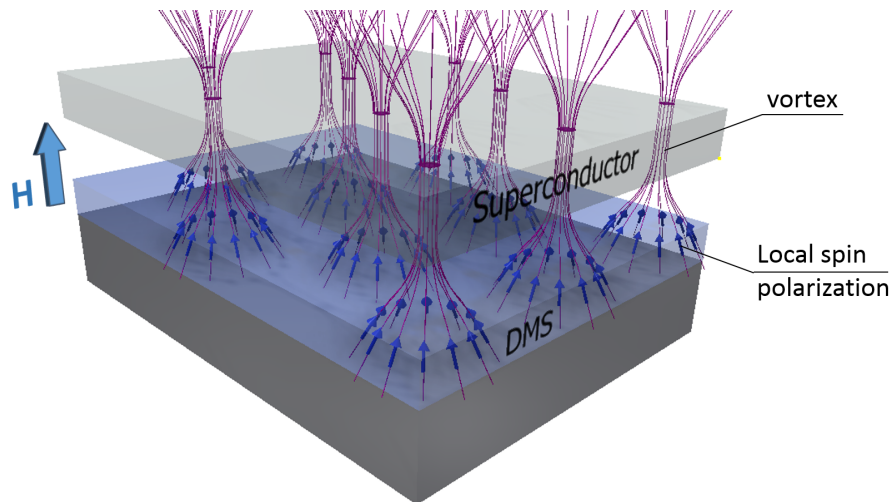


**Figure 1.** Schematic representation of the spin and charge textures created by the stray field of vortices lying in a superconducting layer into a DMS, as theoretically proposed in Reference [19]. The field inhomogeneity of the vortex state is imprinted onto the DMS layer. Spin and charge textures are trapped in the high-field regions inside the DMS.

### 3. Damping of Flux Motion Caused by a Nearby Magnetic Layer

Besides the electromagnetic damping produced by a conducting layer [28–31], in 2007 Palau and co-workers experimentally demonstrated that an additional damping mechanism appears due to the interaction of magnetic flux lines with ferromagnetic particles [32]. In a sample consisting of ferromagnetic Gd nanoparticles (crystallite size of <10 nm) embedded in an Nb film, marked hysteresis with substantial temperature dependence was observed in transport critical current vs magnetic field ( $J_c$  vs  $H$ ). This behaviour appeared when the magnetic field was swept from a value above  $H_{c2}$  of Nb and large enough to saturate the moments of the Gd nanoparticles. Large enhancement in critical current density ( $\Delta J_c \sim 1 \times 10^{10} \text{ A m}^{-2}$ ), and consequently vortex pinning, was observed under such conditions. In contrast to earlier studies of systems with ferromagnetic particles embedded in a superconductor [33–35], the effect was attributed to a new pinning mechanism, ‘magnetic hysteresis pinning’, related to changes in the effective field on the Gd nanoparticles due to displacement of vortices in the Nb. Since in Nb, the magnetic flux is confined within vortices, the field experienced by a Gd nanoparticle is higher if it lies within a vortex than outside it. Thus, the ferromagnetic moment of the nanoparticles is perturbed by changes in the vortex position, as illustrated in Figure 2. The hysteresis in the magnetization of the Gd nanoparticles generates losses, and consequently, the flux motion in the superconductor is damped.

A similar damping mechanism is expected to occur in situations where a ferromagnetic layer is placed on top of a superconducting film. In such a system, the magnetic stray field of vortices travelling across the superconductor induces a co-moving magnetic polarization in the ferromagnetic material. The local magnetization changes following a minor hysteresis cycle, resulting in a drag force similar to that experienced by a permanent magnet moving along a ferromagnetic thin strip [36]. Extrapolating the results of the magnet/thin strip case to the motion of a single vortex, the magnetic hysteresis drag force is expected to be independent on the vortex velocity and proportional to both the ferromagnetic layer thickness and the lateral extension of the vortex stray magnetic field,  $L_{\text{lat}} \sim \lambda$  (assuming that the characteristic length of the microstructure of the ferromagnetic material is smaller than  $L_{\text{lat}}$ ). Such parametric dependence was also observed in the Gd/Nb films of Reference [32]. The strength of the drag force is further determined by the hysteresis processes in the ferromagnetic layer, which are associated with irreversible domain wall displacements in most ferromagnetic materials. In contrast, materials commercially used for magnetic recording are optimized in order to obtain small magnetic grains (of a few nm size) separated by well defined domain walls, with a strong reduction of the exchange coupling and the magnetic interaction between the grains [37]. As a result, the magnetization reversal is dominated by the rotation of the local magnetic moments, which is a reversible process for field strengths much smaller than the coercivity (several hundred mT) [38]. Although residual hysteresis losses may arise from other mechanisms related to the complex structure of the magnetic recording materials, the net hysteresis drag force is expected to be small in such materials.

More recently, an additional damping mechanism consisting in the emission of magnons has been identified theoretically by Beshpalov and co-workers [39]. A moving vortex lattice in a superconductor interacting with magnetic moments in a ferromagnetic layer is accompanied by an ac magnetic field which leads to magnon generation [39,40]. In such systems, transport characteristics of ideal and disordered vortex lattices driven by a dc force are proposed to feature resonance peaks on current-voltage characteristics and step-like increase in current at some critical voltage, respectively. The emission of magnons, which results in a drag force, starts when a Cherenkov resonance condition is satisfied. The damping mechanism is thus present for high vortex velocities  $v > v_{\text{th}}$ , where the threshold velocity  $v_{\text{th}}$  is estimated in the range  $10^3$ – $10^5$  m/s for U-based compounds. Such damping mechanism might hence be relevant for the highest vortex velocities which are commonly observed in thermomagnetic flux avalanches and can reach  $\sim 10^4$ – $10^5$  m/s. Experimental evidence of vortex-magnon interaction have been recently reported in Nb/FeNi structures [41].

Another mechanism leading to a magnetic damping of vortex motion was investigated by Lin and Bulaevskii for the case of a magnetic multilayer system with a large magnetic susceptibility and a long magnetization relaxation time [42]. The magnetic interaction between the superconductor and the magnetic layers was shown to generate polarons, composed of the vortices and their co-moving non-uniform magnetization. In such systems, polarons form at small velocities, for which they experience an enhanced viscosity, while they dissociate as velocity increases thus lowering the magnetic viscosity as a result of this decoupling. Last, vortices driven at very high velocities may trigger additional excitations in the system, leading to an enhanced damping. For instance, vortices exceeding the velocity of sound can trigger Cherenkov-type hypersound emission [43,44]. In addition, at such high velocities, an escape of normal quasiparticles from the vortex core may also lead to the Larkin-Ovchinnikov instability with a sudden transition to a more dissipative state [45].

The determination of the different regimes of vortex flow damping thus necessitates a careful analysis of the magnetic coupling between the superconductor and the magnetic sub-system. In particular, one must consider the relevant system excitations for the considered velocity range, be it smooth magnetic penetration for the lowest velocities or sudden bursts of magnetic flux occurring in avalanches.



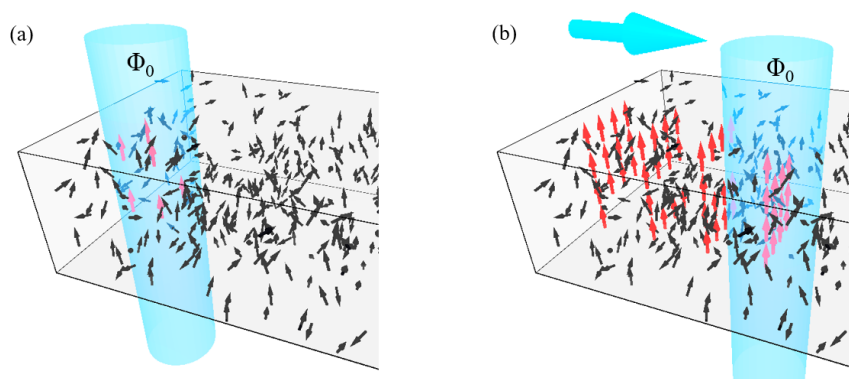


**Figure 2.** Schematic representation showing ferromagnetic particles enclosed in and around a vortex. (a) Local magnetic moments inside the flux line get polarized along the direction of magnetic field (red arrows), while those outside it retain a random orientation (black arrows). (b) Changes induced in the nanoparticle moments, leaving a wake of polarized moments along the path of the vortex.

#### 4. Tracking the Flux Penetration Footsteps by Magnetic Imprinting

In the previous section we have shown how a magnetic medium with low coercive field could affect the motion of flux lines. We now turn our attention to the other side of the coin, i.e., the modification induced in the magnetic medium as a consequence of the vortex motion.

Local polarization of a magnetic material has been a widespread and reliable tool for data storage, as utilized in hard disk drives and magnetic stripe cards. In a magnetic drawing board, which works under the same principle, a magnetic tip attracts and drags along its path magnetic particles in the board (cf. Figure 3a for a model scenario of a magnet dragging iron fillings along with it). The study in Reference [32] suggests the intriguing possibility of locally polarizing a ferromagnetic material in the vicinity of a vortex via its stray field. That is, the principle presented in Figure 3a can be extended to the case of using the flux lines in a superconductor as microscopic magnetic scribes to manipulate the polarization of a soft ferromagnetic layer by the stray fields associated with the flux lines (cf. schematic in Figure 3b). A fascinating proposition is that the polarization thus, induced at cryogenic temperatures could be retained up to room temperature, and for long enough to be characterized further, thus allowing analysis of the flux distribution in a superconductor *ex-situ* by conventional techniques such as magnetic force microscopy.

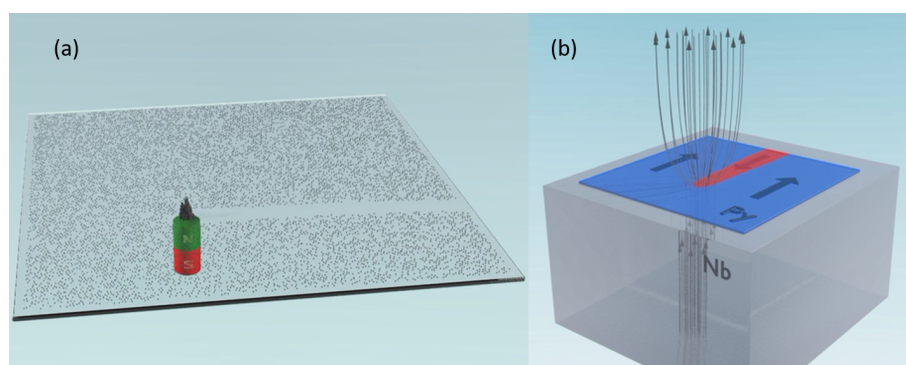


**Figure 3.** (a) A travelling magnet attracts iron fillings on its way and leaves a trail marking its trajectory. (b) A superconducting vortex in motion flips the polarization of a soft ferromagnetic layer in its vicinity and leaves a magnetic imprinting along its path (cf. Section 4.2 for details).

#### 4.1. Techniques to Detect Magnetic Recording of Superconducting States

Magneto-optical imaging (MOI) is a magnetic field mapping technique which has proven to be useful for investigation of ferromagnets as well as superconductors [46–48]. It is characterized by limited invasiveness [30,31,49], short acquisition time [50,51], and reasonable spatial and magnetic field resolution. In particular, a major advantage of MOI over scanning probe magnetic imaging techniques (such as scanning Hall probe microscopy (SHPM) and magnetic force microscopy (MFM)) is the ability to quickly map the magnetic field profile over extended areas (up to few mm). Over the years, the technique has been utilized to various ends; achieving single vortex resolution [49,52–54] and detecting large area phenomena such as flux avalanches in superconductors [55,56]. This technique has been successfully used [56,57] to trace flux trajectories in superconductors by magnetic imprinting.

While MOI enables detection and analysis of the out-of-plane component of magnetic field, another phenomenon, X-ray magnetic circular dichroism (XMCD) [58], has been recently applied to detect and analyse the in-plane components of the magnetic moment. While the spatial resolution of the MOI technique is ultimately limited by the wavelength of the used visible light, microscopy methods based on XMCD overcome this limitation by replacing visible light with soft X-ray and offer enhanced spatial resolution by utilizing scanning X-ray microscopy [59–62]. The complementarity of both techniques has indeed been demonstrated in [60] where magnetic X-ray microscopy images based on XMCD and magneto-optical images have revealed the in-plane and out-of-plane field components in YBCO films under similar conditions.

Although MOI and XMCD have been the techniques of choice for mapping the imprinted magnetic state above the superconducting critical temperature, many other alternative experimental methods able to probe the local magnetic field distribution could be used with the purpose of improving the spatial and field resolution. A non-exhaustive list includes scanning electron microscopy with polarized analysis [63], Kerr microscopy [64], Bitter decoration [65,66], Lorentz microscopy [67], scanning probe microscopy where the probe can be a magnetic tip [68], a Hall cross [69], a nanoSQUID [70], or a nitrogen-vacancy center [71], just to name a few.

#### 4.2. Observation of Imprinted Flux Trajectories in Permalloy Using MOI

Recently, Brisbois and co-authors have demonstrated the imprinting of superconducting vortex trajectories in a magnetic layer [56] of Permalloy ( $\text{Fe}_{19}\text{Ni}_{81}$ , henceforth referred to as Py) on top of a superconducting Nb film, separated by a thin insulating  $\text{SiO}_2$  layer in order to reduce proximity effects and thus, to ensure purely magnetic interaction between the Py and Nb layers (cf. schematic in Figure 4a). A number of such Py/Nb heterostructures were prepared, with different thicknesses of the Py layer ( $t = 50$  nm, 100 nm, and 460 nm). The heterostructures were investigated primarily using MOI (see Reference [72] for more details on the MOI setup). The magnetic landscape in these samples has been found to be highly re-configurable by imprinting flexible micromagnet structures for guidance of flux penetration in a superconductor [56,72].

The magnetic stray field emerging from the superconductor can induce magnetic moment flipping in a ferromagnetic layer if the volume of the latter, and hence, its associated magnetic energy, is small enough. This was indeed observed in heterostructures with thin Py layers ( $t = 50$  nm and 100 nm), in which the vortex trajectories in the Nb left their imprints in the Py layer. The Py layer is polarized in-plane in a particular direction, and a moving flux front with the in-plane field component in the opposite direction is able to flip the local polarization of Py, leaving in its wake a trail of reversed polarization in the Py layer (as schematically represented in Figure 3b).

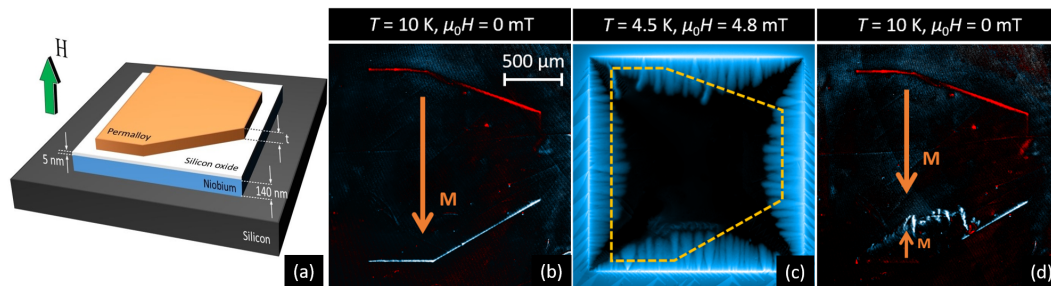


**Figure 4.** (a) Schematic representation of the Py/Nb heterostructures used in Reference [56]. (b) MO image at  $T = 10$  K showing the Py/Nb sample with a 50 nm-thick layer magnetized in-plane, with the magnetization direction indicated by the arrow. (c) MO image at  $T = 4.5$  K and  $\mu_0 H = 4.8$  mT, showing smooth flux penetration in Nb. After obtaining the image (c), the temperature is increased to  $T = 10$  K and  $\mu_0 H = 0$  mT, resulting in the image in panel (d). Panel (d) shows clear reversal of the in-plane magnetisation induced by flux penetration. Figure reprinted from Reference [56].

Figure 4b shows a MO image of the sample at 10 K, above the critical temperature  $T_c$  of Nb, after applying and removing an in-plane field of 10 mT. The in-plane magnetization of the Py is along the direction indicated by the arrow and the stray field of the magnetic layer is clearly visible as white/blue (positive field) and red (negative field) stripes. Subsequently, the sample is cooled to 4.5 K and an out-of-plane field of 4.8 mT is applied. Smooth flux penetration in Nb is observed to remain nearly unaffected by the magnetic layer, as shown in Figure 4c. The temperature is then increased to 10 K and the out-of-plane field is reduced to zero. A MO image captured in this state reveals a striking feature: clear imprints of flux paths in the Nb layer are observed close to one of the borders in the Py layer at 10 K (cf. Figure 4d). In Reference [56] it was argued that the in-plane field component associated with the flux front is strong enough to flip locally the magnetic moments of the Py layer, and this moment-flipping is responsible for the observed imprints. The situation is as shown earlier schematically in Figure 3b, and this also explains the observation that such imprints are not seen at other borders of the Py layer where the in-plane field components are not antiparallel to the local magnetic moment.

More interesting imprinting features are revealed at lower temperatures. Figure 5 summarizes observations following a protocol similar to those discussed in Figure 4, at  $T = 4$  K, for which the Nb sample is in the thermomagnetic instability regime. In addition to velocity-dependent electromagnetic damping [30,31], in this case, flux avalanches are observed to be damped due to the energy cost of flipping in-plane moments in Py when propagating anti-parallel to them (cf. in-plane magnetization orientation in Py shown in panels (a) and (d) and corresponding propagation of flux avalanches in Nb shown in panels (b) and (e) of Figure 5, respectively). Furthermore, the remnant MO signal after warming up to 10 K (cf. panels (c) and (f)) clearly shows traces of the flux trajectories in Nb left in the Py layer. Indeed, using image analysis in Reference [56] very good spatial correlation between flux avalanches in Figure 5b,e and their imprints in Figure 5c,f, respectively, has been established.

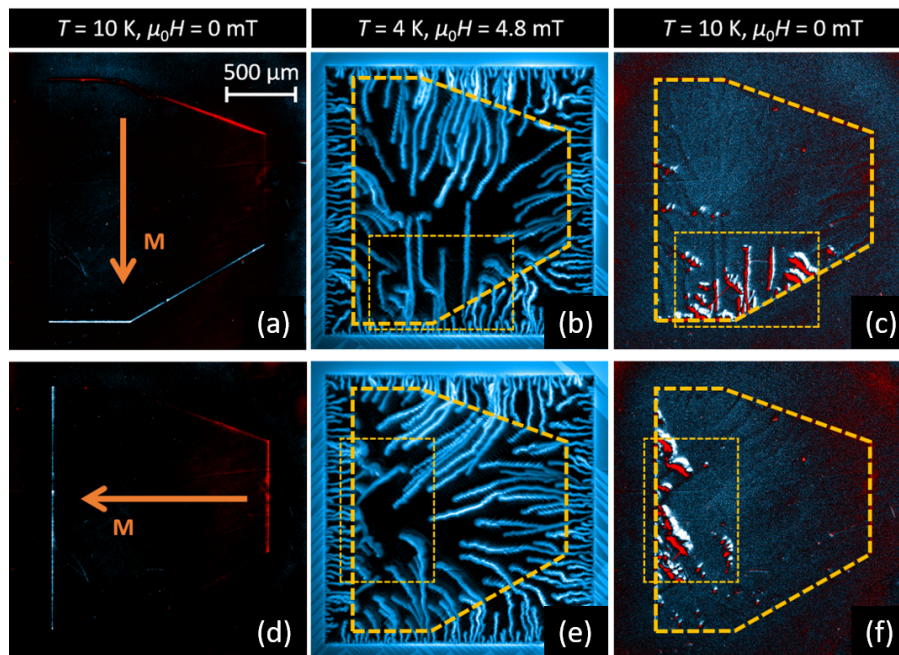


**Figure 5.** (a) MO image at  $T = 10$  K showing the Py/Nb sample with 50 nm-thick Py layer magnetized in-plane, with the magnetization direction indicated by the arrow. (b) MO image at  $T = 4$  K and  $\mu_0 H = 4.8$  mT, showing flux penetration in the form of thermomagnetic avalanches in Nb. (c) MO image at  $T = 10$  K and  $\mu_0 H = 0$  mT, showing imprints of the flux avalanches in Nb visible in the Py layer. (d–f) Set of images similar to those shown in (a–c), with a different initial magnetization direction of Py indicated by the arrow in (d). Figure reprinted from Reference [56].

Recently, Colauto and co-workers have demonstrated [73] that vortices in Nb thin films can be guided by vortices in the plane of the film created by in-plane external magnetic fields above the in-plane lower critical field ( $H_{c1}^{\parallel}$ ). In principle, this scenario could also take place in the Py/Nb heterostructures, as the superconductor is cooled down in the stray field generated by the Py layer. If so, these in-plane vortices could represent an additional mechanism for the preferential propagation of flux along the direction of magnetization of the Py layer, as observed in panels (b) and (e) of Figure 5. The in-plane lower critical field for the Nb film considered in Figure 5 can be estimated [73,74] as  $H_{c1}^{\parallel} \approx 88$  mT. This value largely exceeds the in-plane component of the stray field generated by the Py film at a distance  $\sim 5$  nm as determined from an analytical solution valid for a parallelepiped magnetic layer [75]. In view of this fact, the scenario of frozen-in in-plane vortices does not seem to be relevant in this particular case.

The imprinting of the inhomogeneous magnetic landscape generated by the superconducting layer should not be limited to magnetic layers with preferential in-plane magnetic moment. To address this issue, we have used a magnetic layer already optimized for the storage of information with high density: a hard disk drive (HDD) platter. In recent HDDs, out-of-plane magnetization (confirmed by bulk magnetization measurements, data not shown) allows to record more information in less space. Using these materials represents a first approach towards improving the resolution of magnetic flux imprinting, possibly even down to the single vortex resolution. In particular, we used a Seagate Barracuda T500LM030 HDD platter as magnetic film and deposited a 100 nm-thick rectangular Nb film on top of it, as shown in Figure 6a,b. Following a similar procedure as in Figures 4 and 5, the MO images presented in Figure 6c,d (resp. Figure 6e,f) show that imprinting of some flux avalanches triggered in the Nb film at 2.5 K after cooling in zero field (ZFC) (resp. FC), is retained in the HDD layer at 10 K. Strikingly, these preliminary results show similar imprinting as in the in-plane magnetic moment films. Considering the fact that an HDD involves a complex multilayer structure with the presence of a soft underlayer made of highly permeable material, one is led to admit that flux avalanches in the



superconductor may not be able to induce switching in the out-of-plane recording media, but leave an imprint into the soft underlayer instead.

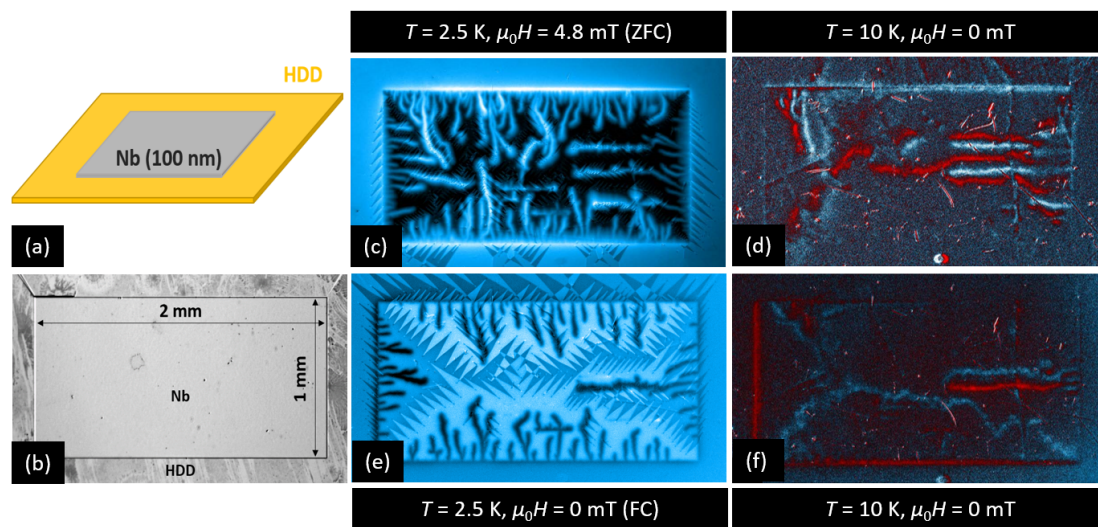


**Figure 6.** (a) Layout of the Nb-HDD sample, consisting of a Seagate Barracuda ST500LM030 hard drive, relying on the perpendicular magnetic recording technology, and a 100 nm-thick Nb superconducting film. (b) Optical image of the sample layout. (c) MO image at  $T = 2.5$  K and  $\mu_0 H = 4.8$  mT, showing flux penetration in the form of thermomagnetic avalanches in Nb after cooling the sample in zero field (ZFC). (e) MO image at  $T = 2.5$  K and  $\mu_0 H = 0$  mT, showing the remnant flux in Nb after withdrawing the applied magnetic field  $\mu_0 H = 4.8$  mT (FC procedure). (d,f) MO images at  $T = 10$  K and  $\mu_0 H = 0$  mT, showing imprints of the flux avalanches in Nb visible in the HDD layer, after the ZFC and FC procedures, respectively.

#### 4.3. Observation of Imprinted Flux Trajectories in Co Using MOI

Similar imprinting of magnetic flux paths in a superconductor to generate unconventional spin textures in ferromagnetic layers has been reported in Nb/Al<sub>2</sub>O<sub>3</sub>/Co thin film heterostructures by Lopes and co-workers [57]. After zero field cooling the sample from above  $T_c$  of Nb to  $T = 2.5$  K, the magnetic flux is observed to penetrate in the form of several dendrite structures (cf. MO image at  $T = 2.5$  K and  $\mu_0 H = 6$  mT in Figure 7a). Upon removing the applied magnetic field and warming up the sample above  $T_c$ , the flux avalanches in Nb are observed to have left their trails in the Co layer, as observed in the MO image at 10 K in Figure 7b, showing the flux distribution in the remanent state of the Co layer, which exhibits a striking correspondence with the flux paths in panel (a). In the MO image at  $T = 300$  K (Figure 7c), the imprints are indeed still present, although there appears to be some washing out of the magnetic textures as compared to those at  $T = 10$  K, which could perhaps be attributed to clustering of domains in the Co film. Hence, the magnetic texture observed at 10 K is found to be reasonably stable even at room temperature, and is expected to be stable up to the Curie temperature of the Co film. It is worth noting that, in principle, the particular thickness of Co film used in the study would allow only for stable domains with in-plane magnetization [76]. Moreover, it is estimated that the magnetic energy provided by the flux front in Nb to the Co film may not be sufficient to induce spin-flipping [77]. Rather than that, it is speculated in Reference [57] that, at the microscopic scale, the observed magnetization texture could result from the formation of skyrmions or some other non-conventional spin chiral-type or vortex-type structures.



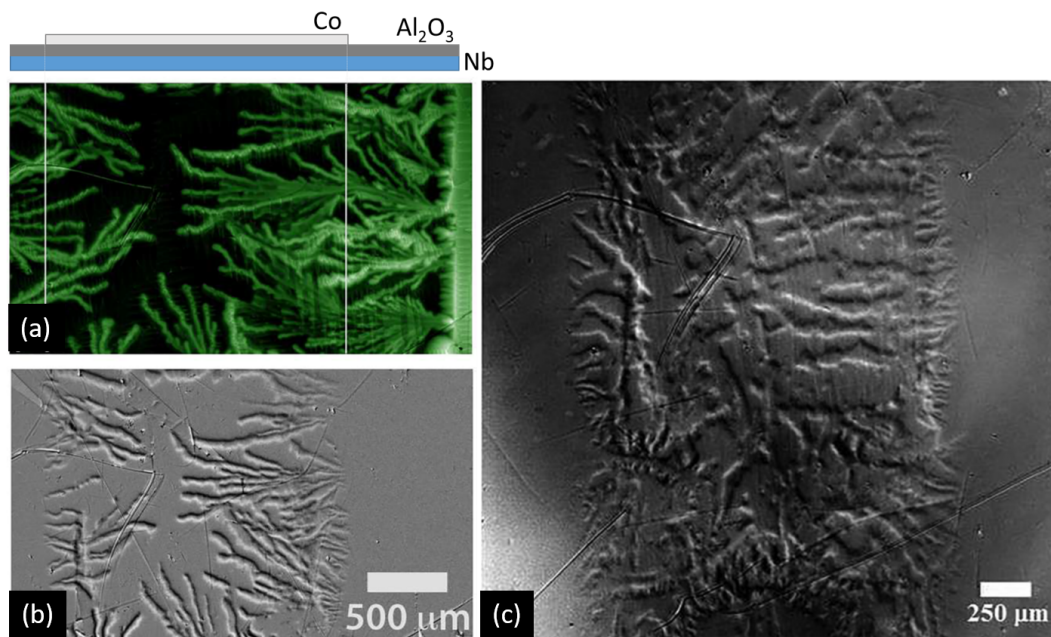


**Figure 7.** (a) MO image at  $T = 2.5$  K and  $\mu_0 H = 6$  mT of the Nb/Al<sub>2</sub>O<sub>3</sub>/Co heterostructures used in Reference [57] showing flux avalanches inside the sample forming a dendritic morphology. The gray vertical lines delineate the region covered with the Co layer. The schematic above panel (a) shows a side view indicating the borders of the Co and Al<sub>2</sub>O<sub>3</sub> layers in the MO image. (b) Remanent state of the Co layer at  $T = 10$  K. (c) MO image at  $T = 300$  K showing imprints of the flux avalanches in the Co layer. Figure reprinted from Reference [57], with permission from AIP Publishing, 2019.

#### 4.4. Imprinting of Inhomogeneous Magnetic Landscapes in CoFeB Detected by XMCD Based Imaging Techniques

The MOI technique is not particularly suited for direct measurements of superconductors and some magnetic materials for which the Faraday effect is very weak. Instead, it is necessary to place a Faraday-active sensor on top of the sample of interest to achieve the desired results. Similarly, the XMCD technique cannot be used directly to characterize superconductors due to absence of paramagnetic ions [59]. Therefore, an additional sensor layer has to be introduced. Maximum magnetic contrast can be achieved by directly depositing the sensor layer on the superconductor (or other sample of interest).

Albrecht and co-workers have reported on XMCD microscopy of magnetic flux patterns in the high- $T_c$  superconductor YBCO (YBa<sub>2</sub>Cu<sub>3</sub>O<sub>7- $\delta$</sub> ) using 30 nm-thick soft ferromagnetic Co<sub>40</sub>Fe<sub>40</sub>B<sub>20</sub> (CoFeB) directly deposited on YBCO as a sensor layer [59–61]. Both optimally doped YBCO thin films (thickness 100–150 nm) and melt-textured YBCO (thickness 350  $\mu$ m) have been studied (cf. schematics in Figure 8a). The XMCD effect is the difference of two X-ray absorption spectra (XAS) obtained using left and right circularly polarized light. In these studies, X-ray beams are tuned to the L<sub>3</sub>-edge of Co, and hence, the resultant contrast corresponds directly to the magnetic moment of the element.

In such CoFeB films, the magnetic moments are found to be oriented in-plane and they exhibit soft ferromagnetic behaviour characterized by small coercive fields ( $\mu_0 H_c = 5$  mT). In these studies, it was demonstrated that by virtue of its soft magnetic nature, CoFeB can act as a recording medium for flux patterns in YBCO. Figure 8b,c show the distribution of the in-plane magnetic flux in one such YBCO thin films with CoFeB cover. The MO image in panel (b) is obtained using the principle discussed in Reference [59]. The scanning X-ray microscopy in panel (c) clearly demonstrates the utility of the CoFeB layer as a recording medium for the flux distribution in YBCO, as the magnetic domains which persist at room temperature have a striking resemblance to the superconducting state at low temperatures. Figure 8d,g demonstrate the additional advantage of enhanced spatial resolution of this technique in comparison with MOI. It is seen that the magnetic contrast in CoFeB at room temperature,

replicating the superconducting state at low temperatures, can be resolved down to 130 nm which is close to the domain wall width ( $\approx 150$  nm) in ferromagnetic (Fe,Co,B)-systems [78].

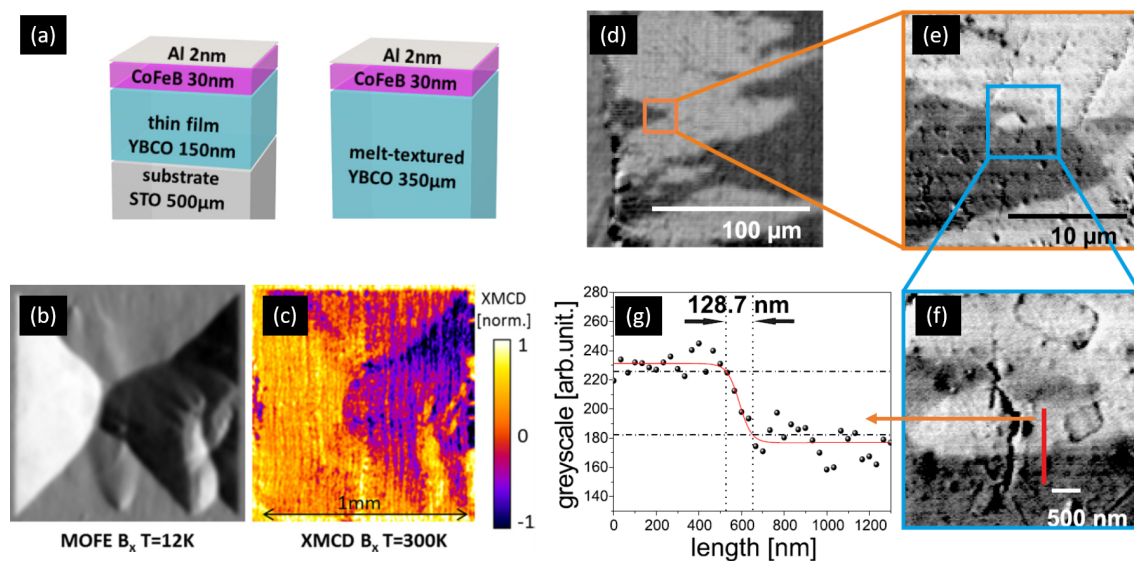


**Figure 8.** (a) Schematic representations of the heterostructures of CoFeB with YBCO thin film and melt-textured YBCO studied in References [59–61]. (b) Magneto-optical image based on the Faraday effect at  $T = 12$  K showing the in-plane magnetic flux distribution  $B_x$  of the critical state of a YBCO thin film covered with CoFeB. (c) XMCD image at  $T = 300$  K showing signatures of the flux distribution in YBCO present in CoFeB at room temperature. (d–f) XMCD images of melt-textured YBCO with CoFeB at room temperature at various magnifications showing imprints in CoFeB of the flux distribution in YBCO at  $T = 83$  K. (g) Line profile along the red line shown in (f), demonstrating the spatial resolution of the technique. Figure reprinted from References [59], with permission from American Physical Society, 2014; References [60], with permission from AIP Publishing, 2015; References [61], with permission from AIP Publishing, 2015.

#### 4.5. Imprinting of Inhomogeneous Magnetic Landscapes in Permalloy Detected by XMCD Based Imaging Techniques

The XMCD technique has also been used for the investigation of recording of magnetic flux patterns in YBCO in an adjacent Permalloy sensor layer [79,80]. Figure 9a shows a schematic of a heterostructure investigated by transmission X-ray microscopy, which consists of the layer of interest, i.e., optimally doped YBCO film epitaxially grown on single crystalline  $\text{SrTiO}_3$  (001) (STO) with Py as a sensor layer on top. The image in Figure 9b shows magnetic (XMCD) signal in the remanent state of YBCO obtained using this technique. In this state, supercurrents in the superconducting layer form four domains of constant current density. This electric current distribution produces in-plane components of the magnetic flux density at the magnetic layer that are oriented towards the edge of the film (Figure 9c). The XMCD image clearly shows the expected pattern of in-plane components of the magnetic flux density in this state, and hence, demonstrates the efficient recording of the superconducting signal in the Py sensor layer.

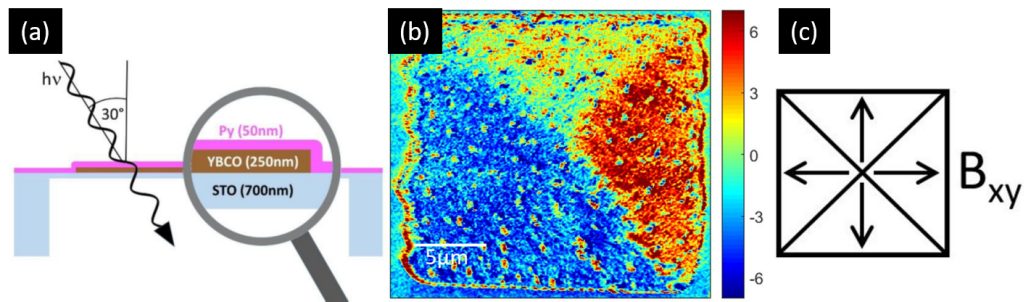


**Figure 9.** (a) Schematic drawing of the Py-YBCO heterostructures studied in Reference [79]. Imaging is performed utilizing transmission of X-ray incident at an angle of  $30^\circ$ . (b) Image of YBCO in the remanent state at  $T = 20$  K obtained by magnetic X-ray microscopy. (c) Sketch of the in-plane magnetic field distribution at the ferromagnetic layer, generated by the supercurrents. Figure reprinted from Reference [79], with permission from American Physical Society, 2018.

XMCD has been also utilized in X-ray photoelectron emission microscopy (X-PEEM) to image in-plane magnetic domain configurations in Py induced by underlying YBCO dots [62]. Figure 10a shows SEM images of different samples geometries investigated. Panels (b) and (c) of Figure 10 show XMCD images which reveal the remanent state of YBCO at 45 K in the form of a clear modulation of the Py magnetization guided by the YBCO layer underneath. Similarly to MOI investigation of Py superconductor heterostructures in Reference [56], it has been demonstrated in Reference [62] that the magnetic history experienced by the Py/YBCO hybrid controls the ultimate magnetic pattern imprinted in the Py layer and that such flexible imprinting can be done in a controllable manner.

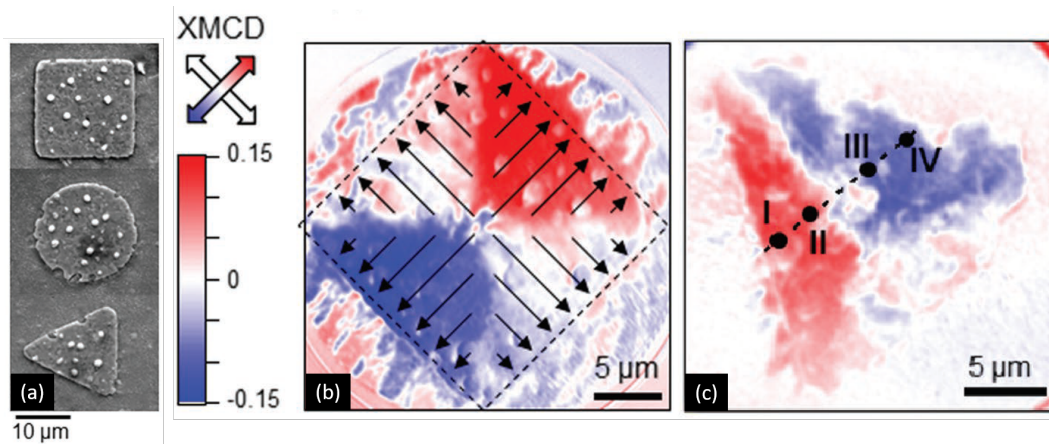


**Figure 10.** (a) Scanning Electron Microscopy (SEM) image of Py-YBCO hybrid structures with different YBCO dot geometry (square, disk, and triangle) studied in Reference [62]. (b,c) XMCD images of Py layer on top of a square and triangular YBCO dot, respectively, obtained at  $T = 45$  K at remanence after maximum applied field (+30 mT and -30 mT, respectively). Figure reprinted from Reference [62], with permission from authors, 2016.

## 5. Conclusions and Outlook

To summarize, we have presented the currently available experimental evidence of imprinting in a ferromagnetic layer the inhomogeneous magnetic landscapes generated by a superconductor. Although the feasibility of the approach has been corroborated by various experimental techniques, a complete understanding of the resulting magnetically recorded state is still lacking. In particular, the differences between the expected imprinting performed in out-of-plane vs in-plane ferromagnetic layers deserve further systematic investigation. The sensitivity of the ferromagnetic layer, in units of mT, can be defined as the minimum local magnetic field threshold required to generate a well-defined feature in it. This quantity may be linked to the coercivity of the magnetic material. The resolution



(in nm) corresponds to the smallest feature of a given type that can be printed and may result from a complex interplay of magnetic film thickness, coercive field and remanent moment. Finally, the contrast corresponds to the magnetic moment gradient from a magnetically exposed area to an unexposed area of the ferromagnetic layer. In this case, a square magnetic loop with well defined coercivity and remanent moment will exhibit binary imprinting, whereas canted moments will permit obtaining a more greyscale imprinting. Part of the appeal of the technique arises from the persistence of the imprinted magnetic landscape up to room temperature so as to be comfortably inspected *ex-situ*. In turn, this requires magnetic materials with Curie temperatures above room temperature. The optimization of sensitivity, resolution, contrast, stability, recording density, etc. within a complex multi-parameter space continues to be an active subject of technological research for magnetic recording of hard-disk drives operating at room temperature. Nowadays, recording densities as high as 1 Tbit/inch<sup>2</sup> can be obtained [81], suggesting that individual flux quantum imaging limit could be reached with the magnetic imprinting technique, at least at low fields (<50 mT) where the local field modulation amplitude is larger. Although much can be learnt from the colossal work done for optimizing magnetic recording in hard disk drives, extrapolating the acquired knowledge on these information storage devices to cryogenic temperatures is not straightforward since most of the parameters are temperature dependent. A particular disadvantage of the magnetic imprinting technique is its invasiveness due to the mutual magnetic interaction between superconductors and ferromagnets. This effect can be minimized if the local field of individual flux quanta (Equation (1)) largely exceeds the coercive field of the ferromagnetic layer. In order to reduce the coercivity, thinner ferromagnetic layers could be used [82,83], at the expense of reducing the Curie temperature [84]. Furthermore, optimization of the parameters for imprinting nearly isothermal and stable states, such as the superconducting critical state, imposes different constraints than those needed for imprinting magnetic flux avalanches in superconductors which can substantially heat the material locally and propagate at speeds exceeding those of magnetic domains [85]. Although in the present review we have focused our attention to the achievements obtained using conventional ferromagnetic as recording layer, alternative materials like half-metallic ferromagnets [86], magnetic topological insulators [87], and ferromagnetic Weyl semimetals [88] might provide fertile ground for the development of the next-generation of magnetic recording of the superconducting states. Clearly, further theoretical and experimental efforts are needed to permit this emerging technique to advance from the current proof-of-concept stage to a mature level.

**Funding:** The authors thank the Fonds de la Recherche Scientifique—FNRS and the COST programme NanoCoHybri. The LANEF framework (ANR-10-LABX-51-01) and the Nanoscience Foundation are acknowledged for their support with mutualized infrastructure. The work of S.B.A. and A.V.S. is partially supported by PDR T.0106.16 of the F.R.S.-FNRS. J.B., B.V., and A.V.S. acknowledge the support of the ARC grant 13/18-08 for Concerted Research Actions, financed by the French Community of Belgium (Wallonia-Brussels Federation). The work of G.S. is supported by the University of Liège and the EU in the context of the FP7-PEOPLE-COFUND-BeIPD project. The authors acknowledge Yves-Eric Corbisier for the sketches displayed in Figure 3. This work was supported in part by the São Paulo Research Foundation (FAPESP) under Grant 2007/08072-0, in part by the National Council for Scientific and Technological Development (CNPq), in part by the Coordenação de Aperfeiçoamento de Pessoal de Nível Superior—Brasil (CAPES)—Finance Code 001.

**Conflicts of Interest:** The authors declare no conflict of interest.

## References

1. Buzdin, A.I. Proximity effects in superconductor-ferromagnet heterostructures. *Rev. Mod. Phys.* **2005**, *77*, 935–976. [[CrossRef](#)]
2. Lyuksyutov, I.F.; Pokrovsky, V.L. Ferromagnet-superconductor hybrids. *Adv. Phys.* **2005**, *54*, 67–136. [[CrossRef](#)]
3. Aladyshkin, A.Y.; Silhanek, A.V.; Gillijns, W.; Moshchalkov, V.V. Nucleation of superconductivity and vortex matter in superconductor–ferromagnet hybrids. *Supercond. Sci. Technol.* **2009**, *22*, 053001. [[CrossRef](#)]

4. Fertig, W.A.; Johnston, D.C.; DeLong, L.E.; McCallum, R.W.; Maple, M.B.; Matthias, B.T. Destruction of Superconductivity at the Onset of Long-Range Magnetic Order in the Compound  $\text{ErRh}_4\text{B}_4$ . *Phys. Rev. Lett.* **1977**, *38*, 987–990. [[CrossRef](#)]
5. Ishikawa, M.; Fischer, Ø. Destruction of superconductivity by magnetic ordering in  $\text{Ho}_{1.2}\text{Mo}_6\text{S}_8$ . *Solid State Commun.* **1977**, *23*, 37–39. [[CrossRef](#)]
6. Canfield, P.; Bud'ko, S.; Cho, B. Possible co-existence of superconductivity and weak ferromagnetism in  $\text{ErNi}_2\text{B}_2\text{C}$ . *Phys. C Supercond.* **1996**, *262*, 249–254. [[CrossRef](#)]
7. Saxena, S.S.; Agarwal, P.; Ahilan, K.; Grosche, F.M.; Haselwimmer, R.K.W.; Steiner, M.J.; Pugh, E.; Walker, I.R.; Julian, S.R.; Monthoux, P.; et al. Superconductivity on the border of itinerant-electron ferromagnetism in  $\text{UGe}_2$ . *Nature* **2000**, *406*, 587–592. [[CrossRef](#)]
8. Aoki, D.; Huxley, A.; Ressouche, E.; Braithwaite, D.; Flouquet, J.; Brison, J.P.; Lhotel, E.; Paulsen, C. Coexistence of superconductivity and ferromagnetism in  $\text{URhGe}$ . *Nature* **2001**, *413*, 613. [[CrossRef](#)]
9. Lee, P.A.; Nagaosa, N.; Wen, X.G. Doping a Mott insulator: Physics of high-temperature superconductivity. *Rev. Mod. Phys.* **2006**, *78*, 17. [[CrossRef](#)]
10. Pathak, S.; Shenoy, V.B.; Randeria, M.; Trivedi, N. Competition between Antiferromagnetic and Superconducting States, Electron-Hole Doping Asymmetry, and Fermi-Surface Topology in High Temperature Superconductors. *Phys. Rev. Lett.* **2009**, *102*, 027002. [[CrossRef](#)]
11. Devizorova, Z.; Mironov, S.; Buzdin, A. Theory of Magnetic Domain Phases in Ferromagnetic Superconductors. *Phys. Rev. Lett.* **2019**, *122*. [[CrossRef](#)] [[PubMed](#)]
12. Tamegai, T.; Nakao, Y.; Nakajima, Y. Shrinkage of magnetic domains in superconductor/ferro-magnet bilayer. *J. Phys. Conf. Ser.* **2009**, *150*, 052263. [[CrossRef](#)]
13. Aladyshkin, A.Y.; Buzdin, A.I.; Fraerman, A.A.; Mel'nikov, A.S.; Ryzhov, D.A.; Sokolov, A.V. Domain-wall superconductivity in hybrid superconductor-ferromagnet structures. *Phys. Rev. B* **2003**, *68*, 184508. [[CrossRef](#)]
14. Pannetier, B.; Rodts, S.; Genicon, J.L.; Otani, Y.; Nozieres, J.P. Macroscopic Quantum Phenomena and Coherence in Superconducting Networks. In *Macroscopic Quantum Phenomena and Coherence in Superconducting Networks*; Giovannella, C.; Tinkham, M., Eds.; World Scientific: Singapore, 1996; pp. 17–24. [[CrossRef](#)]
15. Yang, Z.; Lange, M.; Volodin, A.; Szymczak, R.; Moshchalkov, V.V. Domain-wall superconductivity in superconductor-ferromagnet hybrids. *Nat. Mater.* **2004**, *3*, 793. [[CrossRef](#)] [[PubMed](#)]
16. Gömory, F.; Solovyov, M.; Šouc, J.; Navau, C.; Prat-Camps, J.; Sanchez, A. Experimental Realization of a Magnetic Cloak. *Science* **2012**, *335*, 1466–1468. [[CrossRef](#)] [[PubMed](#)]
17. Vélez, M.; Martín, J.; Villegas, J.; Hoffmann, A.; González, E.; Vicent, J.; Schuller, I.K. Superconducting vortex pinning with artificial magnetic nanostructures. *J. Magn. Magn. Mater.* **2008**, *320*, 2547–2562. [[CrossRef](#)]
18. Jafri, H.M.; Ma, X.; Huang, H.; Zhao, C.; Qazi, H.I.A.; Kazmi, S.B.F.; Liu, Z.; Liu, L.; Shi, S.Q.; Li, Y. Current assisted memory effect in superconductor-ferromagnet bilayers: A potential candidate for memristors. *Supercond. Sci. Technol.* **2019**, *32*, 095002. [[CrossRef](#)]
19. Berciu, M.; Rappoport, T.G.; Jankó, B. Manipulating spin and charge in magnetic semiconductors using superconducting vortices. *Nature* **2005**, *435*, 71–75. [[CrossRef](#)]
20. Furdyna, J.K. Diluted magnetic semiconductors. *J. Appl. Phys.* **1988**, *64*, R29–R64. [[CrossRef](#)]
21. Chang, A.M.; Hallen, H.D.; Harriott, L.; Hess, H.F.; Kao, H.L.; Kwo, J.; Miller, R.E.; Wolfe, R.; van der Ziel, J.; Chang, T.Y. Scanning Hall probe microscopy. *Appl. Phys. Lett.* **1992**, *61*, 1974–1976. [[CrossRef](#)]
22. Brisbois, J.; Raes, B.; de Vondel, J.V.; Moshchalkov, V.V.; Silhanek, A.V. Determination of the magnetic penetration depth in a superconducting Pb film. *J. Appl. Phys.* **2014**, *115*, 103906. [[CrossRef](#)]
23. Berciu, M.; Jankó, B. Nanoscale Zeeman Localization of Charge Carriers in Diluted Magnetic Semiconductor-Permalloy Hybrids. *Phys. Rev. Lett.* **2003**, *90*, 246804. [[CrossRef](#)] [[PubMed](#)]
24. Redliński, P.; Wojtowicz, T.; Rappoport, T.G.; Libál, A.; Furdyna, J.K.; Jankó, B. Zero- and one-dimensional magnetic traps for quasiparticles in diluted magnetic semiconductors. *Phys. Rev. B* **2005**, *72*, 085209. [[CrossRef](#)]
25. Redliński, P.; Rappoport, T.G.; Libal, A.; Furdyna, J.K.; Jankó, B.; Wojtowicz, T. Optical response of a ferromagnetic-diluted magnetic semiconductor hybrid structure. *Appl. Phys. Lett.* **2005**, *86*, 113103. [[CrossRef](#)]



26. Betthausen, C.; Dollinger, T.; Saarikoski, H.; Kolkovsky, V.; Karczewski, G.; Wojtowicz, T.; Richter, K.; Weiss, D. Spin-Transistor Action via Tunable Landau-Zener Transitions. *Science* **2012**, *337*, 324–327. [[CrossRef](#)] [[PubMed](#)]
27. Kruihof, G.H.; van Son, P.C.; Klapwijk, T.M. Interaction between moving flux lines and a two-dimensional electron gas. *Phys. Rev. Lett.* **1991**, *67*, 2725–2728. [[CrossRef](#)] [[PubMed](#)]
28. Danckwerts, M.; Goñi, A.R.; Thomsen, C.; Eberl, K.; Rojo, A.G. Enhanced Vortex Damping by Eddy Currents in Superconductor-Semiconductor Hybrids. *Phys. Rev. Lett.* **2000**, *84*, 3702–3705. [[CrossRef](#)]
29. Colauto, F.; Choi, E.; Lee, J.Y.; Lee, S.I.; Patiño, E.J.; Blamire, M.G.; Johansen, T.H.; Ortiz, W.A. Suppression of flux avalanches in superconducting films by electromagnetic braking. *Appl. Phys. Lett.* **2010**, *96*, 092512. [[CrossRef](#)]
30. Brisbois, J.; Vanderheyden, B.; Colauto, F.; Motta, M.; Ortiz, W.A.; Fritzsche, J.; Nguyen, N.D.; Hackens, B.; Adami, O.A.; Silhanek, A. Classical analogy for the deflection of flux avalanches by a metallic layer. *New J. Phys.* **2014**, *16*, 103003. [[CrossRef](#)]
31. Brisbois, J.; Gladilin, V.N.; Tempere, J.; Devreese, J.T.; Moshchalkov, V.V.; Colauto, F.; Motta, M.; Johansen, T.H.; Fritzsche, J.; Adami, O.A.; et al. Flux penetration in a superconducting film partially capped with a conducting layer. *Phys. Rev. B* **2017**, *95*, 094506. [[CrossRef](#)]
32. Palau, A.; Parvaneh, H.; Stelmashenko, N.A.; Wang, H.; Macmanus-Driscoll, J.L.; Blamire, M.G. Hysteretic Vortex Pinning in Superconductor-Ferromagnet Nanocomposites. *Phys. Rev. Lett.* **2007**, *98*, 117003. [[CrossRef](#)] [[PubMed](#)]
33. Rizzo, N.D.; Wang, J.Q.; Prober, D.E.; Motowidlo, L.R.; Zeitlin, B.A. Ferromagnetic artificial pinning centers in superconducting Nb<sub>0.36</sub>Ti<sub>0.64</sub> wires. *Appl. Phys. Lett.* **1996**, *69*, 2285–2287. [[CrossRef](#)]
34. Bael, M.J.V.; Temst, K.; Moshchalkov, V.V.; Bruynseraede, Y. Magnetic properties of submicron Co islands and their use as artificial pinning centers. *Phys. Rev. B* **1999**, *59*, 14674–14679. [[CrossRef](#)]
35. Snezhko, A.; Prozorov, T.; Prozorov, R. Magnetic nanoparticles as efficient bulk pinning centers in type-II superconductors. *Phys. Rev. B* **2005**, *71*, 024527. [[CrossRef](#)]
36. Garshelis, I.J.; Tollens, S.P.L.; Kari, R.J.; Vandenbossche, L.P.; Dupré, L.R. Drag force measurement: A means for determining hysteresis loss. *J. Appl. Phys.* **2006**, *99*, 08D910. [[CrossRef](#)]
37. Piramanayagam, S.N. Perpendicular recording media for hard disk drives. *J. Appl. Phys.* **2007**, *102*, 011301. [[CrossRef](#)]
38. Stoner, E.C.; Wohlfarth, E.P. A Mechanism of Magnetic Hysteresis in Heterogeneous Alloys. *Philos. Trans. R. Soc. A* **1948**, *240*, 599–642. [[CrossRef](#)]
39. Bepalov, A.A.; Mel'nikov, A.S.; Buzdin, A.I. Magnon radiation by moving Abrikosov vortices in ferromagnetic superconductors and superconductor-ferromagnet multilayers. *Phys. Rev. B* **2014**, *89*, 054516. [[CrossRef](#)]
40. Bulaevskii, L.N.; Hruška, M.; Maley, M.P. Spectroscopy of Magnetic Excitations in Magnetic Superconductors Using Vortex Motion. *Phys. Rev. Lett.* **2005**, *95*, 207002. [[CrossRef](#)]
41. Dobrovolskiy, O.V.; Sachser, R.; Brächer, T.; Böttcher, T.; Kruglyak, V.V.; Vovk, R.V.; Shklovskij, V.A.; Huth, M.; Hillebrands, B.; Chumak, A.V. Magnon-fluxon interaction in a ferromagnet/superconductor heterostructure. *Nat. Phys.* **2019**, *15*, 477–482. [[CrossRef](#)]
42. Lin, S.Z.; Bulaevskii, L.N. Enhancement of critical current density in superconducting/magnetic multilayers with slow magnetic relaxation dynamics and large magnetic susceptibility. *Phys. Rev. B* **2012**, *86*, 064523. [[CrossRef](#)]
43. Ivlev, B.I.; Mejía-Rosales, S.; Kunchur, M.N. Cherenkov resonances in vortex dissipation in superconductors. *Phys. Rev. B* **1999**, *60*, 12419–12423. [[CrossRef](#)]
44. Bulaevskii, L.N.; Chudnovsky, E.M. Sound generation by the vortex flow in type-II superconductors. *Phys. Rev. B* **2005**, *72*, 094518. [[CrossRef](#)]
45. Larkin, A.I.; Ovchinnikov, Y.N. Nonlinear conductivity of superconductors in the mixed state. *Sov. J. Exp. Theor. Phys.* **1975**, *41*, 960.
46. McCord, J. Progress in magnetic domain observation by advanced magneto-optical microscopy. *J. Phys. D Appl. Phys.* **2015**, *48*, 333001. [[CrossRef](#)]
47. Jooss, C.; Albrecht, J.; Kuhn, H.; Leonhardt, S.; Kronmüller, H. Magneto-optical studies of current distributions in high-*T<sub>c</sub>* superconductors. *Rep. Prog. Phys.* **2002**, *65*, 651–788. [[CrossRef](#)]

48. Johansen, T.H.; Shantsev, D.V. (Eds.) *Magneto-Optical Imaging*; Springer Science + Business Media: New York, NY, USA, 2004. [[CrossRef](#)]
49. Goa, P.; Hauglin, H.; Olsen, Å.A.; Baziljevich, M.; Johansen, T. Magneto-optical imaging setup for single vortex observation. *Rev. Sci. Instrum.* **2003**, *74*, 141–146. [[CrossRef](#)]
50. Koblishka, M.; Wijngaarden, R. Magneto-optical investigations of superconductors. *Supercond. Sci. Technol.* **1995**, *8*, 199. [[CrossRef](#)]
51. Bending, S.J. Local magnetic probes of superconductors. *Adv. Phys.* **1999**, *48*, 449–535. [[CrossRef](#)]
52. Goa, P.E.; Hauglin, H.; Baziljevich, M.; Il'yashenko, E.; Gammel, P.L.; Johansen, T.H. Real-time magneto-optical imaging of vortices in superconducting NbSe<sub>2</sub>. *Supercond. Sci. Technol.* **2001**, *14*, 729–731. [[CrossRef](#)]
53. Golubchik, D.; Polturak, E.; Koren, G.; Lipson, S.G. A high resolution magneto-optical system for imaging of individual magnetic flux quanta. *Opt. Express* **2009**, *17*, 16160–16165. [[CrossRef](#)]
54. Veshchunov, I.S.; Magrini, W.; Mironov, S.V.; Godin, A.G.; Trebbia, J.B.; Buzdin, A.I.; Tamarat, P.; Lounis, B. Optical manipulation of single flux quanta. *Nat. Commun.* **2016**, *7*, 12801. [[CrossRef](#)] [[PubMed](#)]
55. Johansen, T.H.; Baziljevich, M.; Shantsev, D.V.; Goa, P.E.; Peirin, Y.M.G.; Kang, W.N.; Kim, H.J.; Choi, E.M.; Kim, M.S.; Lee, S.I. Dendritic magnetic instability in superconducting MgB<sub>2</sub> films. *Europhys. Lett. (EPL)* **2002**, *59*, 599–605. [[CrossRef](#)]
56. Brisbois, J.; Motta, M.; Avila, J.I.; Shaw, G.; Devillers, T.; Dempsey, N.M.; Veerapandian, S.K.P.; Colson, P.; Vanderheyden, B.; Vanderbemden, P.; et al. Imprinting superconducting vortex footsteps in a magnetic layer. *Sci. Rep.* **2016**, *6*, 27159. [[CrossRef](#)] [[PubMed](#)]
57. Lopes, R.F.; Carmo, D.; Colauto, F.; Ortiz, W.A.; de Andrade, A.M.H.; Johansen, T.H.; Baggio-Saitovitch, E.; Pureur, P. Spin texture on top of flux avalanches in Nb/Al<sub>2</sub>O<sub>3</sub>/Co thin film heterostructures. *J. Appl. Phys.* **2017**, *121*, 013905. [[CrossRef](#)]
58. Schütz, G.; Wagner, W.; Wilhelm, W.; Kienle, P.; Zeller, R.; Frahm, R.; Materlik, G. Absorption of circularly polarized x rays in iron. *Phys. Rev. Lett.* **1987**, *58*, 737–740. [[CrossRef](#)] [[PubMed](#)]
59. Stahl, C.; Audehm, P.; Gräfe, J.; Ruoff, S.; Weigand, M.; Schmidt, M.; Treiber, S.; Bechtel, M.; Goering, E.; Schütz, G.; et al. Detecting magnetic flux distributions in superconductors with polarized X rays. *Phys. Rev. B* **2014**, *90*, 104515. [[CrossRef](#)]
60. Stahl, C.; Ruoff, S.; Weigand, M.; Bechtel, M.; Schütz, G.; Albrecht, J. Low temperature X-ray imaging of magnetic flux patterns in high temperature superconductors. *J. Appl. Phys.* **2015**, *117*, 17D109. [[CrossRef](#)]
61. Ruoff, S.; Stahl, C.; Weigand, M.; Schütz, G.; Albrecht, J. High-resolution dichroic imaging of magnetic flux distributions in superconductors with scanning x-ray microscopy. *Appl. Phys. Lett.* **2015**, *106*, 022601. [[CrossRef](#)]
62. Palau, A.; Valencia, S.; Del-Valle, N.; Navau, C.; Cialone, M.; Arora, A.; Kronast, F.; Tennant, D.A.; Obradors, X.; Sanchez, A.; et al. Encoding Magnetic States in Monopole-Like Configurations Using Superconducting Dots. *Adv. Sci.* **2016**, *3*, 1600207. [[CrossRef](#)]
63. Scheinfein, M.R.; Unguris, J.; Kelley, M.H.; Pierce, D.T.; Celotta, R.J. Scanning electron microscopy with polarization analysis (SEMPA). *Rev. Sci. Instrum.* **1990**, *61*, 2501–2527. [[CrossRef](#)]
64. Betzig, E.; Trautman, J.K.; Wolfe, R.; Gyorgy, E.M.; Finn, P.L.; Kryder, M.H.; Chang, C.H. Near-field magneto-optics and high density data storage. *Appl. Phys. Lett.* **1992**, *61*, 142–144. [[CrossRef](#)]
65. Grigorieva, I.V. Magnetic flux decoration of type-II superconductors. *Supercond. Sci. Technol.* **1994**, *7*, 161–176. [[CrossRef](#)]
66. Fasano, Y.; Menghini, M. Magnetic-decoration imaging of structural transitions induced in vortex matter. *Supercond. Sci. Technol.* **2008**, *21*, 023001. [[CrossRef](#)]
67. Harada, K.; Matsuda, T.; Kasai, H.; Bonevich, J.E.; Yoshida, T.; Kawabe, U.; Tonomura, A. Vortex configuration and dynamics in Bi<sub>2</sub>Sr<sub>1.8</sub>CaCu<sub>2</sub>O<sub>x</sub> thin films by Lorentz microscopy. *Phys. Rev. Lett.* **1993**, *71*, 3371–3374. [[CrossRef](#)] [[PubMed](#)]
68. Pietzsch, O.; Kubetzka, A.; Haude, D.; Bode, M.; Wiesendanger, R. A low-temperature ultrahigh vacuum scanning tunneling microscope with a split-coil magnet and a rotary motion stepper motor for high spatial resolution studies of surface magnetism. *Rev. Sci. Instrum.* **2000**, *71*, 424–430. [[CrossRef](#)]
69. Kirtley, J.R. Fundamental studies of superconductors using scanning magnetic imaging. *Rep. Prog. Phys.* **2010**, *73*, 126501. [[CrossRef](#)]

70. Finkler, A.; Segev, Y.; Myasoedov, Y.; Rappaport, M.L.; Ne'eman, L.; Vasyukov, D.; Zeldov, E.; Huber, M.E.; Martin, J.; Yacoby, A. Self-Aligned Nanoscale SQUID on a Tip. *Nano Lett.* **2010**, *10*, 1046–1049. [[CrossRef](#)]
71. Acosta, V.M.; Bouchard, L.S.; Budker, D.; Folman, R.; Lenz, T.; Maletinsky, P.; Rohner, D.; Schlusser, Y.; Thiel, L. Color Centers in Diamond as Novel Probes of Superconductivity. *J. Supercond. Novel Magn.* **2018**, *32*, 85–95. [[CrossRef](#)]
72. Shaw, G.; Brisbois, J.; Pinheiro, L.B.G.L.; Müller, J.; Blanco Alvarez, S.; Devillers, T.; Dempsey, N.M.; Scheerder, J.E.; Van de Vondel, J.; Melinte, S.; et al. Quantitative magneto-optical investigation of superconductor/ferromagnet hybrid structures. *Rev. Sci. Instrum.* **2018**, *89*, 023705. [[CrossRef](#)]
73. Colauto, F.; do Carmo, D.; de Andrade, A.M.H.; Oliveira, A.A.M.; Ortiz, W.A.; Galperin, Y.M.; Johansen, T.H. Anisotropic Flux Penetration in Superconducting Nb Films with Frozen-in In-plane Magnetic Fields. *IEEE Trans. Appl. Supercond.* **2019**, *29*, 1–5. [[CrossRef](#)]
74. Abrikosov, A. *Fundamentals of the Theory of Metals*; North Holland: Amsterdam, The Netherlands, 1988.
75. Engel-Herbert, R.; Hesjedal, T. Calculation of the magnetic stray field of a uniaxial magnetic domain. *J. Appl. Phys.* **2005**, *97*, 074504. [[CrossRef](#)]
76. Gil, W.; Görlitz, D.; Horisberger, M.; Kötzler, J. Magnetoresistance anisotropy of polycrystalline cobalt films: Geometrical-size and domain effects. *Phys. Rev. B* **2005**, *72*, 134401. [[CrossRef](#)]
77. Cardarelli, F. *Materials Handbook: A Concise Desktop Reference*, 2nd ed.; Springer: London, UK, 2008. [[CrossRef](#)]
78. Hindmarch, A.T.; Kinane, C.J.; MacKenzie, M.; Chapman, J.N.; Henini, M.; Taylor, D.; Arena, D.A.; Dvorak, J.; Hickey, B.J.; Marrows, C.H. Interface Induced Uniaxial Magnetic Anisotropy in Amorphous CoFeB Films on AlGaAs(001). *Phys. Rev. Lett.* **2008**, *100*, 117201. [[CrossRef](#)] [[PubMed](#)]
79. Simmendinger, J.; Ruoss, S.; Stahl, C.; Weigand, M.; Gräfe, J.; Schütz, G.; Albrecht, J. Transmission X-ray microscopy at low temperatures: Irregular supercurrent flow at small length scales. *Phys. Rev. B* **2018**, *97*, 134515. [[CrossRef](#)]
80. Suszka, A.K.; Gliga, S.; Warnicke, P.; Wintz, S.; Saha, S.; Charipar, K.M.; Kim, H.; Wohlhüter, P.; Kirk, E.; Finizio, S.; et al. Observation of the out-of-plane magnetization in a mesoscopic ferromagnetic structure superjacent to a superconductor. *Appl. Phys. Lett.* **2018**, *113*, 162601. [[CrossRef](#)]
81. Tannous, C.; Comstock, R.L. Magnetic Information-Storage Materials. In *Springer Handbook of Electronic and Photonic Materials*; Kasap, S., Capper, P., Eds.; Springer International Publishing: Cham, Switzerland, 2017; p. 1. [[CrossRef](#)]
82. Akhter, M.A.; Mapps, D.J.; Tan, Y.Q.M.; Petford-Long, A.; Doole, R. Thickness and grain-size dependence of the coercivity in permalloy thin films. *J. Appl. Phys.* **1997**, *81*, 4122–4124. [[CrossRef](#)]
83. Dulal, R.P.; Dahal, B.R.; Forbes, A.; Pegg, I.L.; Philip, J. Large magnetization and high Curie temperature in highly disordered nanoscale Fe<sub>2</sub>CrAl thin films. *J. Magn. Magn. Mater.* **2017**, *423*, 314–317. [[CrossRef](#)]
84. Jensen, P.J.; Dreyssé, H.; Bennemann, K.H. Calculation of the Film-Thickness-Dependence of the Curie Temperature in Thin Transition Metal Films. *Europhys. Lett. (EPL)* **1992**, *18*, 463–468. [[CrossRef](#)]
85. Redjdal, M.; Giusti, J.; Ruane, M.F.; Humphrey, F.B. Thickness dependent wall mobility in thin Permalloy films. *J. Appl. Phys.* **2002**, *91*, 7547. [[CrossRef](#)]
86. Katsnelson, M.I.; Irkhin, V.Y.; Chioncel, L.; Lichtenstein, A.I.; de Groot, R.A. Half-metallic ferromagnets: From band structure to many-body effects. *Rev. Mod. Phys.* **2008**, *80*, 315–378. [[CrossRef](#)]
87. Tokura, Y.; Yasuda, K.; Tsukazaki, A. Magnetic topological insulators. *Nat. Rev. Phys.* **2019**, *1*, 126–143. [[CrossRef](#)]
88. Dulal, R.P.; Dahal, B.R.; Forbes, A.; Bhattarai, N.; Pegg, I.L.; Philip, J. Weak localization and small anomalous Hall conductivity in ferromagnetic Weyl semimetal Co<sub>2</sub>TiGe. *Sci. Rep.* **2019**, *9*, 3342. [[CrossRef](#)] [[PubMed](#)]

